An egalitarian network model for the emergence of simple and complex cells in visual cortex

Louis Tao, Michael Shelley, David McLaughlin, and Robert Shapley

This information is current as of May 2007.

Notes:

An egalitarian network model for the emergence of simple and complex cells in visual cortex

Louis Tao*, Michael Shelley†, David McLaughlin, and Robert Shapley

Courant Institute of Mathematical Sciences, New York University, 251 Mercer Street, New York, NY 10027; and Center for Neural Science, New York University, 4 Washington Place, New York, NY 10003

We explain how simple and complex cells arise in a large-scale neuronal network model of the primary visual cortex of the macaque. Our model consists of ≈4,000 integrate-and-fire, conductance-based point neurons, representing the cells in a small, 1-mm² patch of an input layer of the primary visual cortex. In the model the local connections are isotropic and nonspecific, and convergent input from the lateral geniculate nucleus confers cortical cells with orientation and spatial phase preference. The balance between lateral connections and lateral geniculate nucleus drive determines whether individual neurons in this recurrent circuit are simple or complex. The model reproduces qualitatively the experimentally observed distributions of both extracellular and intracellular measures of simple and complex response.

spatial summation | computational models

A fundamental classification of neurons in the primary visual cortex (V1) is as simple or complex (1). A simple cell responds to visual stimulation in an approximately linear fashion. For example, when responding to the temporal modulation of standing grating patterns, simple cells modulate their firing at the stimulus frequency and are sensitive to its spatial phase (or location). Complex cells are very nonlinear, modulating their firing at twice the stimulus frequency and showing little sensitivity to spatial phase.

Simple and complex cells may have different tasks in visual perception. Cortical cells must represent spatial properties such as surface brightness and color and the perceptual spatial organization of a scene that is the basis of form. Simple cells are necessary for all of these functions because they are the visual cortical neurons that are able to respond monotonically to signed edge contrast. Complex cells, being insensitive to spatial phase, cannot provide a cortical representation of signed contrast, but they are sensitive to texture, firing at elevated rates in response to stimuli within their receptive fields.

Although long-standing and with functional implications, the simple/complex classification is hardly sharp. Recent work by Ringach *et al*. (2) analyzes the extracellular responses of neurons across many experiments in macaque V1. They find that many V1 cells are neither wholly simple nor wholly complex but lie somewhere in between. And although most cells in V1 might be classified as complex, the cortical layer that receives the bulk of lateral geniculate nucleus (LGN) excitation, 4*C*, has simple and complex cells in approximately equal proportion.

Associated with the simple/complex classification is the influential hierarchical model of Hubel and Wiesel (1), shown schematically in Fig. 1*a*, wherein simple cells receive geniculate drive and the pooling of their phase-specific outputs drives the phase invariant responses of complex cells. As we argue in *Results*, this conception seems difficult to reconcile with recent experimental evidence. Chance, Nelson, and Abbott (3) have put forward a very different model that investigates the possible role of recurrent excitation in creating complex cells. In their model, the phase-specific outputs of excitatory simple cells drive cells coupled together in an excitatory recurrent network (Fig. 1*b*). Realizing this architecture by using a rate model for network activity, they find phase invariant, complex

responses when recurrent excitation in the network dominates that of the simple cell inputs.

Here, we study a large-scale model of the neuronal dynamics in layer 4*Cα* of macaque V1, whose architecture is known better than for almost any other cortical area. Our model is egalitarian, in the sense that all neurons interact with each other at the same level, with local lateral connectivity being nonspecific and isotropic (Fig. 1*c*). Previously, we showed how strong network inhibition in a cortical network model could ameliorate the nonlinearities of LGN excitation, and so give rise to a network of simple cells (4). That work also showed that cortico-cortical excitatory conductances resembled the spiking responses of complex cells. Such complex-like responses in membrane conductances of simple cells is consistent with *in vivo* voltage-clamp measurements made by Borg-Graham *et al*. (5) in cat cortical cells after flashed bar stimulation.

Building on this observation, our model cortex naturally produces simple cells, complex cells, and cells with intermediate responses. Although strong cortico-cortical inhibition remains an important feature, a central assumption of this model is that the strength of LGN excitation varies broadly, so that some cortical cells receive significant LGN drive, whereas others receive little. This is combined with the constraint that the total excitatory synaptic drive onto each cell is approximately constant, although divided between geniculate and striate sources, as is suggested by theories of cortical development (6, 7) and by recent experiments (8). Through a balance of strong recurrent excitation and inhibition this model yields complex responses in those cells with relatively little LGN drive. Simple cells arise in a manner similar to those of the earlier Wielaard *et al*. model (4).

The aim of our modeling is to understand the function of the V1 cortical network in terms of network connectivity and dynamics. Thus to be successful, the model must account in a realistic manner for orientation selectivity, response dynamics with a wide range of input stimuli, firing rate patterns in background, as well as during stimulation. All of these aspects of the egalitarian model's performance will be reported elsewhere. In this article, we focus on the model's performance in spatial summation experiments that have been used to classify neurons as simple or complex. We show that this egalitarian model, which combines natural assumptions on the variability of cortical and geniculate drive and what is known about the neuronal architecture of V1, can rationalize many aspects of the available experimental data. The model yields physiologically reasonable simple and complex cell responses, both in the rate and the form of spiking. The architecture leads to distinctive predictions of population measures of simple/complex responses, which have the qualitative structure seen in recent experimental measurements. Our work here may prove important for understanding the roles of network excitation and inhibition in other cortical areas.
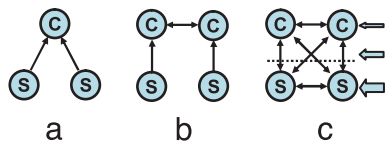
Fig. 1. Schematics of models for complex cells. (*a*) The hierarchical model of Hubel and Wiesel (1), wherein the summed output of simple cells drives complex cells. (*b*) The recurrent excitation model of Chance et al. (3). (*c*) The present egalitarian model where simple and complex cells coexist within a common circuit. The simple cell model of Wielaard et al. (4) is represented by the portion of the schematic below the dashed line. In the first two models, LGN excitation arrives through the simple cells, which then drive the complex cells. In the model discussed here, LGN excitation arrives with varying strength throughout the network, with this strength represented by the arrows on the right of the schematic.

Methods

Our model cortex consists of $\approx$4,000 coupled excitatory and inhibitory integrate-and-fire point neurons, whose intracellular potentials follow:

$$\frac{dv^j}{dt} = -g_L(v^j - V_L) - g_E^j(t)(v^j - V_E) - g_I^j(t)(v^j - V_I)$$

$$= -g_T^j(t)(v^j - V_S^j(t)). \qquad [1]$$

where g_L is the leak conductance; $g_E^j(t)$ and $g_I^j(t)$ are the excitatory and inhibitory conductances, respectively. Here, the conductances have been normalized by the membrane capacitance, leaving them with dimensions of inverse time (e.g., $g_L = 50$ sec^{-1}). V_L, V_E, and V_I are the rest, excitatory, and inhibitory reversal potentials, respectively. In integrate-and-fire dynamics, when the membrane potential hits a threshold, V_T, a spike is recorded and v^j is instan-

taneously reset to V_L. An action potential is associated with a spike time and conductance changes are then distributed throughout the network. Potentials are nondimensional with $V_T = 1$, $V_L = 0$, and by using the commonly accepted values for the various biophysical parameters (9), $V_E = 4.67$, $V_I = -0.67$. In Eq. **1**, $g_T = g_L + g_E^j + g_I^j$ is the total membrane conductance and $V_S^j = (V_E g_E^j + V_I g_I^j)/g_T^j$ is the effective (time-dependent) reversal potential. We use a modified fourth-order Runge–Kutta method (10) with 0.1-ms time steps.

To close the model, we need to specify g_E^j and g_I^j. In short, these conductances are produced by firing activity within the model cortex, from spikes arriving from the LGN, and from spiking of extracortical sources. A major part of the connectivity is described through Fig. 2 and its explication in *Results*, and many further details are given in *Supporting Text*, which is published as supporting information on the PNAS web site.

Results

Contrast Reversal and Spatial Phase Dependence. Contrast reversal is the sinusoidal modulation in time of the contrast of a standing sine-wave pattern. Response to contrast reversal is a critical test of linearity in simple cells (11, 12). A simple cell's response depends strongly on the spatial phase or position of the standing grating pattern relative to the midpoint of the neuron's receptive field and has a large amplitude response at the fundamental driving frequency at one spatial phase (the "preferred phase") and very little response at the "orthogonal phase," 90° away. Response at both of these phases shows little or no generation of the higher temporal harmonics that might be expected for a nonlinear system. On the other hand, nonlinear harmonic distortion products are apparent in the responses of cortical complex cells (11): their temporal responses show little sensitivity to spatial phase, and firing modulates at twice the stimulus frequency (i.e., at the second harmonic).

Simple and complex cell responses, like those seen in experiment,

Fig. 2. Schematic of model. (*Upper*) Inputs from visual stimulation are relayed through the LGN. Each V1 cell "sees" a collection of LGN cells that is probabilistically sampled from a 2D Gabor function. The segregation of convergent on- and off-center LGN cells (represented by red and green circles) confers orientation and spatial phase preference on individual cortical cells; these preferences are inherited from parameters of individual Gabor functions. Orientation preference is laid out in pinwheels (map shown in color), and spatial phase preference is distributed randomly (map not shown, but individual phase preferences are shown for three sample neurons). The number of LGN cells (N_i) providing afferents varies from cell to cell (shown for sample neurons) and is distributed randomly in cortex (uniformly between 0 and 30). The firing rates of individual LGN cells are modeled as inhomogeneous Poisson processes with rates that are taken from a thresholded, linear spatio-temporal filter (as detailed in refs. 4 and 29). (*Lower Left*) Intracortical couplings are isotropic with interaction profiles taken to be Gaussians in space (excitation in red and inhibition in blue), with the length scale of excitation (200 μm) greater than that of inhibition (100 μm). Inhibitory coupling strengths are taken randomly from a Gaussian distribution, whereas excitatory coupling

strengths are drawn from Gaussian distributions whose mean strengths are inversely proportional to N_i. The extra 4Cα conductances have strengths that are also drawn randomly from Gaussian distributions. (*Lower Right*) Each cortico-cortical excitatory postsynaptic potential is taken to be 50% α-amino-3-hydroxy-5-methyl-4-isoxazolepropionic acid (AMPA) and 50% *N*-methyl-D-aspartate (NMDA), whereas an inhibitory postsynaptic potential is divided evenly between γ-aminobutyric acid type A (GABA$_A$) and a slower inhibition [based on recent experimental findings of Gibson et al. (39)].

NEUROSCIENCE
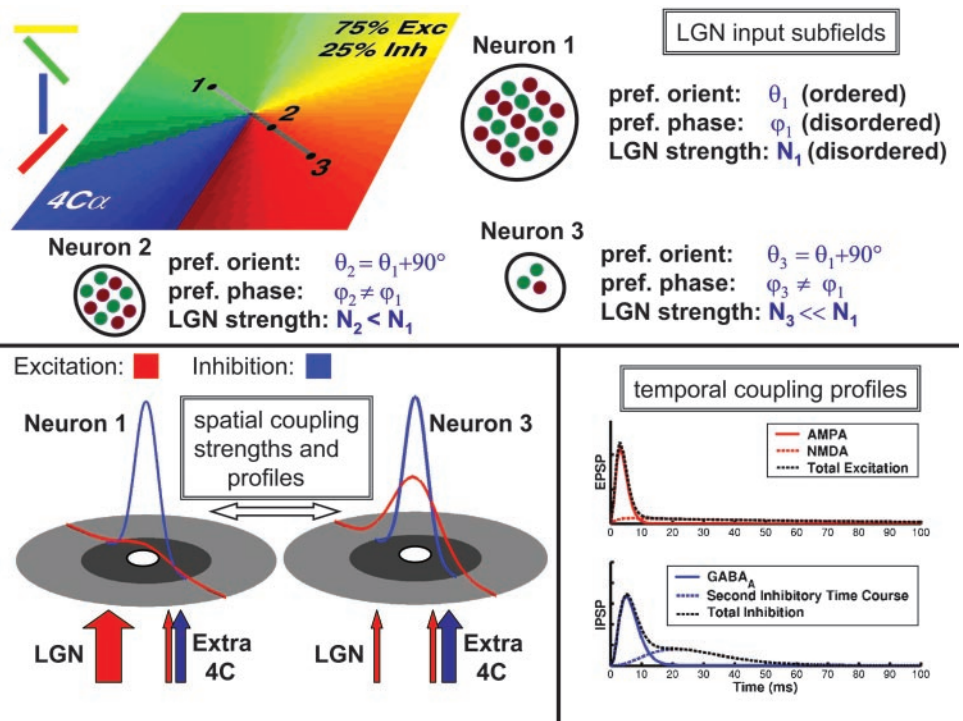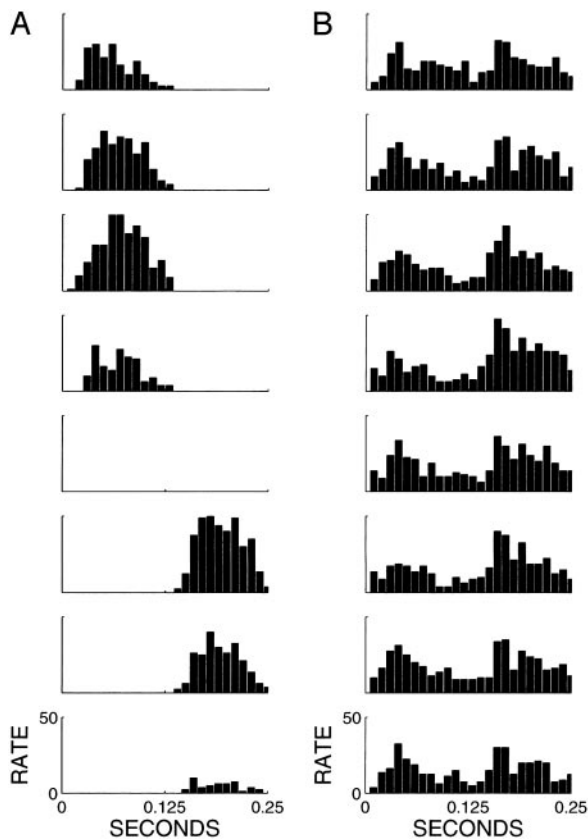
Fig. 3. Responses from model neurons to contrast reversal stimulation (eight spatial phases, at optimal orientation, and temporal and spatial frequency). Shown are predicted responses from a simple (*a*) and a complex (*b*) neuron in the model network. (*a*) Model network simple cell driven at 4 Hz. The spatial phase is defined so that one spatial cycle of the grating pattern is 360°. At 180°, the response is zero. (*b*) Model network complex cell driven at 4 Hz. The response is at the second harmonic and is insensitive to spatial phase.
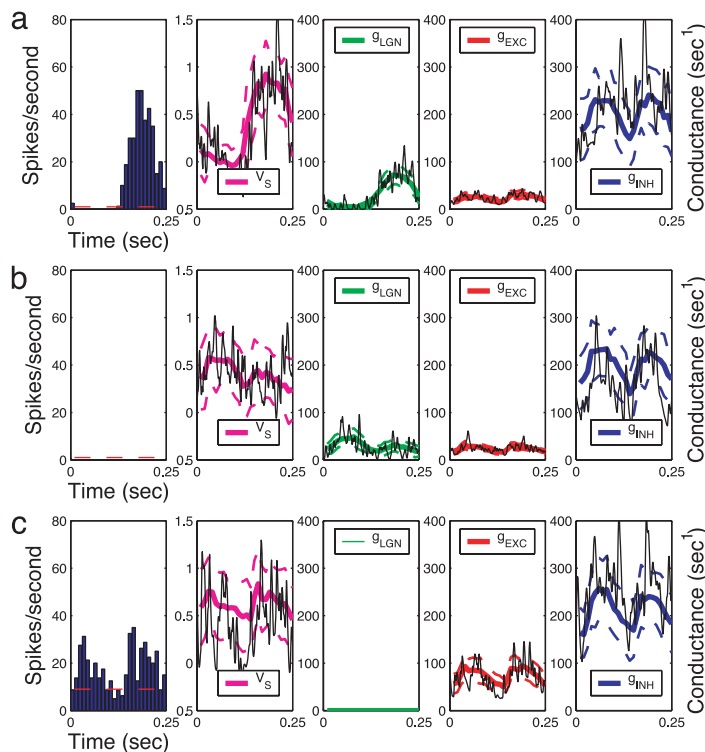
potential V_S (both normalized as described in *Methods*) at the preferred and orthogonal phases of contrast reversal, over one cycle of stimulation. [In our network, the membrane time scale is very short (26), and hence the intracellular potential closely tracks V_S when below the firing threshold, here normalized to unity. When V_S is above unity, the cell is typically firing.] At the preferred phase, the excitatory conductance from the LGN is a rectified sinusoidal wave peaking at three-quarters cycle, whereas at orthogonal phase the LGN excitation is frequency doubled. The latter arises when a zero contrast phase line of the stimulus lies across a segregated subregion of off- or on-centered LGN cells. The stimulus then excites these LGN cells twice in a period, first on one side of the phase line, then on the other, which when combined with the simultaneous firing rectification occurring in LGN cells on the opposing side, yields a frequency doubling (4). Likewise, the rectification nonlinearities of individual LGN cells also yield the half-wave rectified response at the preferred phase. Not shown is the response to the stimulus phase 180° away from the preferred, for which the LGN excitation is nearly identical but peaking instead at one-quarter cycle. Intermediate phases of stimulation appear as combinations of these half-wave rectified and frequency doubled wave forms [see figure 2 of Wielaard *et al*. (4)].

As the spatial phase preference conferred by the LGN drive varies widely from cortical cell to cortical cell, a stimulus phase that is preferred for one cortical cell will for other cells be at preferred, orthogonal, or intermediate phases. For cells with fewer LGN afferents than our model simple cell, all of these basic wave forms of LGN excitation persist, but are diminished in magnitude. An extreme example of this is the sample complex cell, whose intracellular responses are shown in Fig. 4c at the first phase presented in Fig. 3b. This cell has no LGN afferents, and hence no LGN excitation.

Thus, because of the diverse nature of its LGN input, particularly in input phases, the model cortex receives an LGN excitation that for some cells is peaked in the first-half period of stimulation, is peaked in the second half for others, and for yet others is peaked in both halves (i.e., stimulus is at F_2). Consequently, the bulk visual excitation, LGN excitation averaged over all cells, peaks in both halves of the period of stimulation and is insensitive to phase. In a network that is isotropically and nonspecifically coupled, a cell samples through its cortico-cortical conductances the activity of many other cells, each excited by the LGN at a different input phase. A natural consequence is that these conductances reflect the bulk forcing and so are frequency doubled and phase insensitive. This is illustrated in Fig. 4. Both the inhibitory and excitatory cortico-cortical conductances of the simple cell are frequency doubled and practically identical at the two phases shown, as indeed they are also for the other intermediate phases. These observations hold true for the cortico-cortical conductances of the complex cell. Examination at all of its phases of response would show near invariance to phase and frequency doubling.

Tradeoff Between LGN and Cortico-Cortical Input. Phase insensitivity and frequency doubling are key to how this network produces both simple and complex cells. For example, Fig. 4b shows that LGN excitation is frequency doubled at the orthogonal phase, yet this strong nonlinearity in the LGN input is not expressed in the spiking of the cell. As explained in Wielaard *et al*. (4), if excitation and cortico-cortical inhibition are roughly in balance, phase-insensitive cortico-cortical inhibition is sufficient to suppress frequency-doubled firing at the orthogonal phase.

Another structural element of the model network is indicated in Fig. 2. The number of excitatory, LGN afferents driving a cortical cell is inversely correlated to the number of excitatory cortico-cortical afferents. That is, the fewer synapses on a cell taken up by the LGN, the more are available to excitatory (presynaptic) neurons in the network. This assumption is based on theories of cortical development in which the number of excitatory synapses is kept

arise in our model cortex. For contrast reversal stimulation, Fig. 3a shows a model cell responding like a simple cell, and Fig. 3b shows another cell responding like a complex cell. These are but two cells taken from a large-scale network simulation with ≈4,000 cells (75% excitatory, 25% inhibitory). The architecture of this network is presented schematically in Fig. 2. Some of the crucial distinguishing features of the model, derived from biological data, are that the local lateral connectivity is nonspecific and isotropic, with lateral monosynaptic inhibition acting at shorter length scales than excitation (13–16). Orientation and spatial phase preferences are conferred on cortical cells from the convergence of output from many LGN cells (17), with orientation preference laid out in pinwheel patterns (18–21), and spatial phase preference varying widely from cortical cell to cortical cell (22).

As Fig. 2 also indicates, the number of LGN cells, N_{LGN}, whose afferents impinge on a model cortical cell varies broadly and randomly from cortical cell to cortical cell. Much of the evidence for variability in the strength of LGN drive is indirect (23–25), and so for the purposes of this study, we make the simplest assumption and take the distribution of N_{LGN} to be uniform. We have found that changing the precise form of this distribution does not qualitatively change our results. A model simple cell like the cell depicted in Fig. 3a has a nearly maximal number of LGN afferents (conceptually, neuron 1 in the schematic), whereas a complex cell (like the one in Fig. 3b) has few LGN afferents (conceptually neuron 3 in the schematic). Fig. 4 shows the model simple cell's instantaneous and cycle-averaged intracellular conductances and effective reversal

Tao *et al*.

Fig. 4. Extracellular and intracellular responses to 4-Hz contrast reversal. (*a* and *b*) The model simple cell in Fig. 3*a* responding at its preferred and orthogonal spatial phases. (*c*) The model complex cell in Fig. 3*b* at one of the phases. From left to right: cycle-averaged firing rate (with the spontaneous rate in red dashes); effective reversal potential V_S (magenta); LGN-driven conductance (green); cortico-cortical excitatory conductance (red); cortico-cortical inhibitory conductance (blue). Dotted lines are standard deviations for each of the conductances and for the potential. Thin black lines indicate instantaneous values of conductances and potentials. Cycle averages are performed over 24 cycles.

constant (6, 7) [recent experiments support this theoretical constraint (8)]. The consequences of this assumption are made clear in Fig. 4*c*. For the complex cell, the lack of LGN excitation is compensated for by a strong, frequency-doubled cortico-cortical excitation, balanced by likewise frequency-doubled inhibition. The firing pattern of the cell is then naturally frequency-doubled and phase insensitive, as is observed for complex cells.
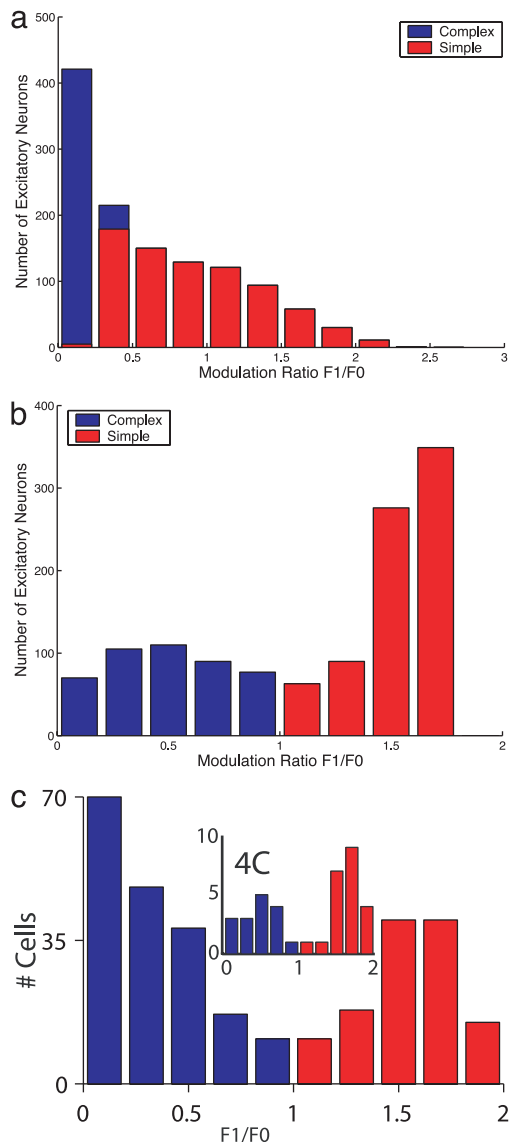
Slow and Fast Excitation. Fig. 2 also illustrates that we use slow excitation in the synapses between cortical cells (see temporal coupling profiles). The total excitatory postsynaptic potential was the sum of an α-amino-3-hydroxy-5-methyl-4-isoxazolepropionic acid (AMPA) component and a *N*-methyl-D-aspartate (NMDA) component (27) with equal weight integrated over time. We found that, in networks where the cortical coupling is mediated only by AMPA, the strong cortical amplification led to large-amplitude

global oscillations. The slow excitation provided by NMDA was necessary to achieve stability in the recurrent network (28). Another feature of this model that differentiates it from Wielaard *et al*. (4) is the presence of a global inhibition and excitation that is modulated by total network activity. This global coupling could be interpreted, for example, as being mediated through layer 6 feedback to layer 4C, and does not affect simple/complex population responses. Its main effect is to improve orientation selectivity within the layer and to remove some of the differences in network activity near and far from the pinwheel centers of orientation hypercolumns [ref. 29; see Kang *et al*. (30) for a recent study of mechanisms underlying neuronal activity patterns in models of the cortical layer].

Drifting Grating Responses. Another common visual stimulus used to classify the response properties of cortical neurons is drifting
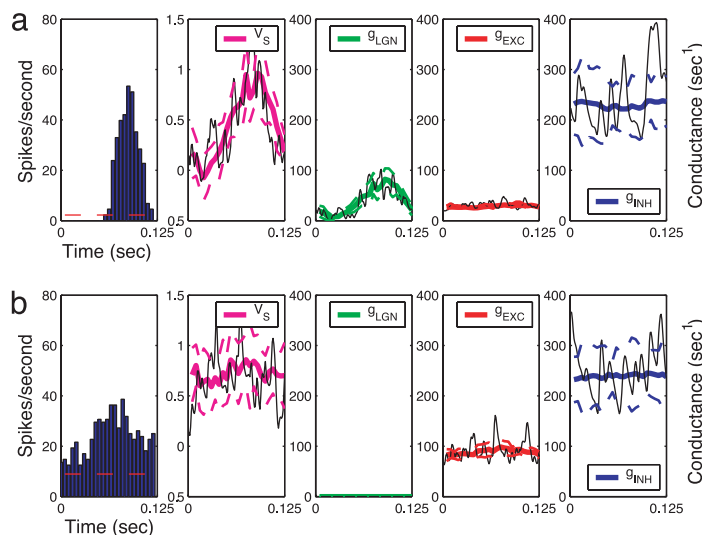
Fig. 5. Responses to 8-Hz drifting grating at optimal orientation. (*a*) The model simple cell in Fig. 3*a*. (*b*) The model complex cell in Fig. 3*b*. From left to right: cycle-averaged firing rates (spontaneous rates as dashed red lines); effective reversal potential V_S (magenta); LGN-driven conductance (green); cortico-cortical excitatory conductance (red); cortico-cortical inhibitory conductance (blue). The dotted lines are standard deviations for each of the conductances and for the potential. The thin black lines indicate instantaneous values of conductances and potentials. Cycle averages are performed over 48 cycles.

NEUROSCIENCE

Fig. 7. Time-averaged conductances as a function of the modulation index F_1/F_0 of the firing rate. Green is LGN-driven conductance, red is cortico-cortical excitation, blue is cortico-cortical inhibition, and black is total conductance. Each point is computed by finding the population of neurons within a certain range in F_1/F_0 and then averaging (over the population and over time). The vertical bars at each point denote the population average of the standard deviation.

Fig. 6. A comparison of intracellular and extracellular F_1/F_0 between model and experiment. (*a*) Distribution of F_1/F_0 of membrane potential (relative to background activity) of excitatory neurons in model network, when stimulated at optimal orientation and spatial frequency. The height of each bar indicates the total number of excitatory neurons in each bin, and the blue and red portions correspond to the cells that are classified as simple or complex based on their extracellular responses. (*b*) Distribution of the modulation ratio F_1/F_0 of the firing rate for excitatory neurons in model network. (The distribution for the inhibitory population is qualitatively similar.) For these two distributions, only cells with mean rates >8 spikes per s are included. (*c*) Distribution of the modulation ratio F_1/F_0 of the firing rate for 308 cells (complex cells, $n = 184$; simple cells, $n = 124$) from the experiments of Ringach *et al.* (2). The detail shows the distribution for the 38 cells identified as being in 4*C*. Here, with a baseline of zero firing rate, the modulation ratio is bounded between zero and two.

sinusoidal gratings (a traveling, spatially modulated intensity pattern, held at a fixed orientation). Although often used to probe selectivities for orientation, frequency, or direction, this stimulus also shows characteristic differences between simple and complex cells. For the model simple and complex cells of Figs. 3 and 4, Fig. 5 shows their extracellular and intracellular responses to a drifting grating stimulus (8 Hz at optimal orientation and spatial frequency). Their extracellular spiking is typical of experimentally observed simple and complex cells. The simple cell follows the temporal modulation of the drifting grating as it moves across its

receptive field, whereas the complex cell shows an elevated, mostly unmodulated firing over the whole cycle of stimulation.

Examination of LGN and cortico-cortical conductances in Fig. 5 accounts for the model's response to drifting gratings. First, the strong LGN excitation into the simple cell modulates with the stimulus frequency. Different cells receive LGN excitation of similar wave form, but because of variability in both the number of LGN afferents and in spatial phase preference, they are diverse in both amplitude and time of peak excitation. For drifting grating stimulation, this yields a bulk forcing to the model cortex that is nearly uniform in time and manifests itself as nearly time-invariant cortico-cortical conductances (4). Thus, for the model simple cell, both the intracellular V_S and its extracellular firing pattern modulate on the time dependence of its LGN input. Conversely, for the model complex cell both V_S and the firing pattern are driven by the unmodulated cortico-cortical conductances, and hence show only elevated, unmodulated responses.

Population Distributions of Modulation Ratio. Given the structure of the model cortex, it is clear that our two sample cells, one simple and one complex, must sit within a continuum of possible intracellular and extracellular responses. We explore this with a standard characterization of response. Fig. 6*a* shows the histogram of modulation ratio F_1/F_0 for the cycle-averaged effective reversal potential, V_S, across the whole population of $\approx 3,000$ excitatory cells within the model cortex. The modulation ratio is the ratio of first harmonic amplitude (at the stimulus frequency) to the mean. Cells with flat intracellular responses, like the sample complex cell in Fig. 5*b*, have small modulation ratios. The distribution of modulation ratio is broad, unimodal, and monotonically decreasing and reflects the broad distribution in the number of LGN afferents and the constraint of fixed, total excitation. In recent unpublished work, David Ferster and colleagues (personal communication) measured the modulation ratio of the intracellular potential for 168 cells in cat cortex (see figure 11 of ref. 31 for an analysis on a much smaller set of cat V1 cells). Like our model here, their measurements show also a broad and unimodal distribution of intracellular F_1/F_0.

Curiously, this unimodality is not preserved in extracellular measures, neither in experiment nor in the model. Fig. 6*b* shows for the model cortex the distribution of modulation ratio of the cycle-averaged firing rate, and Fig. 6*c* shows the measured distri-

butions from Ringach *et al*. (2) for 308 cells in macaque V1 and for the 38 located in 4*C*. Following others (e.g., refs. 2 and 32), we use this extracellular F_1/F_0 as a classifier, labeling as simple those cells with $F_1/F_0 > 1$ (red in Fig. 6*b*), and as complex those with $F_1/F_0 < 1$ (blue in Fig. 6*b*). Qualitatively similar, both distributions show a bimodal structure peaked near the extremes of the classifier but with a large proportion of cells having responses that are neither wholly simple nor wholly complex.

On the basis of a simple model, Mechler and Ringach (33) have recently shown that spike-rate rectification could lead to a bimodal distribution in extracellular F_1/F_0, even though intracellular response is unimodally distributed (see also ref. 34). Our work here shows that this result can arise within a cortical model that incorporates many elements that are biologically realistic. For our model, we note that the form of the intracellular and extracellular F_1/F_0 distributions changed little when the uniform distribution used for N_{LGN}, the number of LGN afferents impinging on a model cortical cell, was replaced by a Gaussian distribution whose standard deviation was half its mean. When the N_{LGN} distribution was made strictly bimodal (half the cortical cells receiving LGN excitation and half receiving none at all), this created an extracellular F_1/F_0 distribution with a greater population of complex cells as seen in Fig. 6*c*, but also a plainly bimodal intracellular distribution.

For the drifting grating stimulus, Fig. 7 shows how membrane conductances relate to extracellular F_1/F_0. First, as expected, the simpler a cell, the stronger its LGN excitation, but it is also true that even very simple cells can receive substantial network excitation. Second, it is clear that LGN and cortico-cortical excitation are generally anticorrelated, with very complex cells receiving almost exclusively cortical excitation. The cortico-cortical inhibition is large and is much more uniform than excitation with respect to F_1/F_0. Finally, across the whole population note that the total conductance is large and is dominated by inhibition [as in Wielaard *et al*. (4)]. Large inhibitory conductances have been found in recent intracellular measurements (35–37), and their effect on cortical function has been studied theoretically (26).

Discussion

The following are the main results of this article. We have constructed a cortical model, based on macaque V1, for the emergence of simple and complex cells within the same basic circuit. Their differing responses reflect differing proportions of geniculate versus cortico-cortical excitation. Although the amount of excitation is kept roughly fixed, its division varies widely from cell to cell, as do many other elements of the model, such as strength of coupling and extracortical drive, and the receptive field properties of convergent LGN excitation. In a manner consistent with experiment measure-

ment, many cells emerge as complex, many as simple, and many as being mixed. We predict a bimodal but broad structure of extracellular modulation ratio, itself arising from a distribution of intracellular modulation ratios that is broad but monotonic. This prediction is consistent with available data.

Our model is very different from the influential hierarchical model of Hubel and Wiesel (1), wherein simple cells receive geniculate drive and their pooled output drives the complex cells. Clearly, a strict rendering of the Hubel and Wiesel model would yield a bimodal population response in both the extracellular and intracellular modulation ratio, as is not observed here, nor in experiment. Our model is more egalitarian than hierarchical, with all cell types receiving strong inputs from the network of both simple and complex cells (see Fig. 7) and with almost all cells receiving LGN drive.

Although our model is motivated by an interpretation of macaque V1 cortical architecture (4, 29) and instantiated in a large-scale computational model with spiking neurons, it shares important features with the modeling of Chance *et al*. (3). As in Chance *et al*., recurrent excitation plays a central role in creating complex cell responses. However, in our model recurrent excitation does not so much play the role of yielding phase invariant responses, as in Chance *et al*., but rather in yielding sufficiently high, physiologically reasonable firing rates for complex cells that are also being inhibited. Phase invariance is built into the complex cell's total synaptic input by summing over both complex cells and simple cells nonspecifically. In an elaboration of their basic model, Chance *et al*. also demonstrated that a mixed population of simple, complex, and intermediate cells could be found by randomly varying the strength of connectivity to the model cortical network.

A crucial feature of our model is cortico-cortical inhibition. Cortical inhibition allows the possibility of nearly linear, simple cell responses in the network, even when driven by LGN cells with their attendant rectification nonlinearities (4).

Finally, we have emphasized in this work the form of the model's cycle- or time-averaged responses. However, examination of Figs. 4 and 5 shows that instantaneous values of V_S and the conductances are strongly fluctuating, with the mean V_S mostly below, or barely above, the threshold to firing. Clearly, fluctuations are important to creating the network state, and as argued in ref. 26, are important to yielding smoothly graded average responses (see also ref. 38).

1. Hubel, D & Wiesel, T. (1962) *J. Physiol. (London)* **160,** 106–154.
2. Ringach, D., Shapley, R. & Hawken, M. (2002) *J. Neurosci.* **22,** 5639–5651.
3. Chance, F., Nelson, S. & Abbott, L. (1999) *Nat. Neurosci.* **2,** 277–282.
4. Wielaard, J., Shelley, M., Shapley, R. & McLaughlin, D. (2001) *J. Neurosci.* **21,** 5203–5211.
5. Borg-Graham, L., Monier, C. & Fregnac, Y. (1996) *J. Physiol. (Paris)* **90,** 185–188.
6. Miller, K. & MacKay, D. (1994) *Neural Comput.* **6,** 100–126.
7. Miller, K. (1996) *Neuron* **17,** 371–374.
8. Royer, S. & Pare, D. (2002) *Neuroscience* **115,** 455–462.
9. Koch, C. (1999) *Biophysics of Computation* (Oxford Univ. Press, Oxford).
10. Shelley, M. & Tao, L. (2001) *J. Comput. Neurosci.* **11,** 111–119.
11. De Valois, R., Albrecht, D. & Thorell, L. (1982) *Vision Res.* **22,** 545–559.
12. Spitzer, H. & Hochstein, S. (1985) *J. Neurophysiol.* **53,** 1244–1265.
13. Fitzpatrick, D., Lund, J. & Blasdel, G. (1985) *J. Neurosci.* **5,** 3329–3349.
14. Lund, J. (1987) *J. Comp. Neurol.* **257,** 60–92.
15. Callaway, E. & Wiser, A. (1996) *Visual Neurosci.* **13,** 907–922.
16. Callaway, E. (1998) *Annu. Rev. Neurosci.* **21,** 47–74.
17. Reid, R. & Alonso, J.-M. (1995) *Nature* **378,** 281–284.
18. Bonhoeffer, T. & Grinvald, A. (1991) *Nature* **353,** 429–431.
19. Blasdel, G. (1992) *J. Neurosci.* **12,** 3115–3138.
20. Blasdel, G. (1992) *J. Neurosci.* **12,** 3139–3161.
21. Maldonado, P., Godecke, I., Gray, C. & Bonhoeffer, T. (1997) *Science* **276,** 1551–1555.
22. DeAngelis, G., Ghose, R., Ohzawa, I. & Freeman, R. (1999) *J. Neurosci.* **19,** 4046–4064.
23. Tanaka, K. (1985) *Vision Res.* **25,** 357–364.
24. Alonso, J.-M., Usrey, W. M. & Reid, R. (2001) *J. Neurosci.* **21,** 4002–4015.
25. Ringach, D. (2002) *J. Neurophysiol.* **88,** 455–463.
26. Shelley, M., McLaughlin, D., Shapley, R. & Wielaard, J. (2002) *J. Comp. Neurosci.* **13,** 93–109.
27. Rivadulla, C., Sharma, J. & Sur, M. (2001) *J. Neurosci.* **21,** 1710–1719.
28. Wang, X. (1999) *J. Neurosci.* **19,** 9587–9603.
29. McLaughlin, D., Shapley, R., Shelley, M. & Wielaard, J. (2000) *Proc. Natl. Acad. Sci. USA* **97,** 8087–8092.
30. Kang, K., Sompolinsky, H. & Shelley, M. (2003) *Proc. Natl. Acad. Sci. USA* **100,** 2848–2853.
31. Carandini, M. & Ferster, D. (2000) *J. Neurosci.* **20,** 470–484.
32. Skottun, B., DeValois, R., Grosof, D., Movshon, J., Albrecht, D. & Bonds, A. (1991) *Vision Res.* **31,** 1079–1086.
33. Mechler, F. & Ringach, D. (2002) *Vision Res.* **42,** 1017–1033.
34. Abbott, L. & Chance, F. (2002) *Nat. Neurosci.* **5,** 391–292.
35. Borg-Graham, L., Monier, C. & Fregnac, Y. (1998) *Nature* **393,** 369–373.
36. Hirsch, J., Alonso, J.-M., Reid, R. & Martinez, L. (1998) *J. Neurosci.* **15,** 9517–9528.
37. Anderson, J., Carandini, M. & Ferster, D. (2000) *J. Neurophysiol.* **84,** 909–926.
38. Anderson, J., Lampl, I., Gillespie, D. & Ferster, D. (2000) *Science* **290,** 1968–1972.
39. Gibson, J., Beierlein, M. & Connors, B. (1999) *Nature* **402,** 75–79.

NEUROSCIENCE